

# Decoupling of Electron and Ion Dynamics in Driven Magnetic Reconnection\* in Collisionless Plasmas<sup>\*)</sup>

C. Z. CHENG, Shizuo INOUE<sup>1)</sup>, Yasushi ONO and Ritoku HORIUCHI<sup>2)</sup>

*School of Frontier Sciences, University of Tokyo, Tokyo 113-8656, Japan*

<sup>1)</sup>*Japan Atomic Energy Agency, Naka 311-0193, Japan*

<sup>2)</sup>*National Institute for Fusion Science, Toki 509-5292, Japan*

(Received 31 December 2015 / Accepted 2 April 2016)

The purpose of the paper is to describe the decoupling processes of electron and ion dynamics in the reconnection layer (current sheet and separatrix regions) and how the in-plane electrostatic electric field and the parallel electric field are produced. During driven magnetic reconnection of oppositely directed magnetic field lines, both ions and electrons drift together with the merging field lines toward the neutral sheet where the magnetic field lines reconnect. Because the electron outflow velocity is much larger than the ion outflow velocity, a pair of currents flow inward toward the magnetic reconnection region and produce the quadrupole out-of-plane magnetic field concentrated around the separatrix regions. The parallel electric field is produced by the driving electric field and the quadrupole magnetic field and points toward the downstream direction. The parallel electric field accelerates electrons toward the reconnection region direction but ions move slowly across the separatrix field lines, which causes decoupling of the electron and ion flow dynamics around the separatrix regions to generate charge separation and produce electrostatic electric field pointing across the separatrix field lines toward the mid-plane direction. Around the magnetic reconnection region where the magnetic fields become weakened and reversed, the particle orbits perpendicular to the field lines become meandering. Because the ion meandering region width is much larger than the electron meandering region width, charge separation is produced inside the ion meandering region and produces a pair of strong bipolar in-plane electrostatic electric fields pointing toward the mid-plane direction. With the production of quadrupole magnetic field, the parallel electric field and the electrostatic electric field, particle dynamics and acceleration/heating can be understood.

© 2016 The Japan Society of Plasma Science and Nuclear Fusion Research

Keywords: magnetic reconnection, kinetic theory, parallel electric field, decoupling of electron-ion dynamics, electron acceleration, ion heating

DOI: 10.1585/pfr.11.1401081

## 1. Introduction

Physics of magnetic reconnection has been studied by using various models and experiments. Based on the MHD model, there are two steady-state magnetic reconnection models: the Sweet-Parker model and the Petschek model. In the Sweet-Parker model, both electrons and ions flow together from the upstream region through the magnetic reconnection diffusion layer into the downstream region and the outflow velocity speeds up to the Alfvén speed by the reconnection electric field. The reconnection rate (or the inflow speed) is proportional to the square root of the plasma resistivity and is too low to explain observations and experimental results. To overcome the problems of slow reconnection rate and inflow bottleneck, the Petschek model proposes that both electrons and ions flow together mainly across the magnetic field line separatrix into the downstream and the plasma outflow velocity is accelerated by the  $\vec{J} \times \vec{B}$  force at the assumed slow mode shock

which is located in the downstream region. Then, the inflow speed can be enhanced to realistic value. On the other hand, based on the Hall-MHD model, the electron flow decouples from the ion flow. The electron flow velocity perpendicular to  $\vec{B}$  is governed by the  $c\vec{E} \times \vec{B}/B^2$  drift velocity, and the ion flow velocity is controlled by the  $\vec{J} \times \vec{B}$  and pressure gradient forces, where  $\vec{J}$  is the plasma current density. However, the charge quasi-neutrality is assumed so that there is no electrostatic electric field. Moreover, the plasma pressure is assumed to be isotropic and obey the adiabatic pressure law, and there is no information on the electron and ion parallel flow velocities along the magnetic field. Also, there is no information on plasma heating and acceleration. The additional feature of the Hall-MHD model is that around the reconnection exhaust region the magnetic field is weak and thus the electron perpendicular outflow velocity ( $c\vec{E} \times \vec{B}/B^2$ ) is larger than the ion perpendicular outflow velocity. Then, a pair of currents inflowing toward the reconnection X-point are formed to generate the quadrupole out-of-plane magnetic field. However, this physical mechanisms of the electron and ion outflow ve-

author's e-mail: frankcheng@k.u-tokyo.ac.jp

\*) This article is based on the invited talk at the 32nd JSPF Annual Meeting (2015, Nagoya)

locities are not correct from the full particle kinetic physics point of view [1].

The kinetic processes of magnetic reconnection based on the full kinetic model are drastically different from those based on the MHD and Hall-MHD models. In this paper we first explain how the quadrupole out-of-plane magnetic field, the parallel electric field are produced. Then, we discuss the physical processes that cause the decoupling of the electron and ion dynamics, which lead to the generation of the charge separation and the in-plane electrostatic electric field. The key kinetic physics of driven magnetic reconnection of anti-parallel magnetic fields in collisionless plasmas presented in this paper are obtained by examining the 2-1/2 dimensional particle-in-cell simulation results [1, 2]. We also discuss the similarities and differences of the physical mechanisms between the driven reconnection results presented in this paper and the previously published results of undriven (or spontaneous) reconnection simulations.

## 2. Simulation Parameters

In the simulations, the electron and ion thermal speeds are defined as  $v_{Te} = (T_e/m_e)^{1/2}$  and  $v_{Ti} = (T_i/m_i)^{1/2}$ , where  $T_e$ ,  $T_i$ ,  $m_i$  and  $m_e$  are the initial electron and ion temperatures and masses, respectively. The electron and ion plasma frequencies  $\omega_{pe} = (4\pi n_{e0}e^2/m_e)^{1/2}$  and  $\omega_{pi} = (4\pi n_{e0}e^2/m_i)^{1/2}$ , the electron Debye length  $\lambda_{De} = v_{Te}/\omega_{pe}$  and the ion skin depth  $\lambda_{di} = c/\omega_{pi}$  are defined with the electron density at the initial Harris current sheet location. The electron and ion cyclotron frequencies  $\omega_{ce} = eB_0/m_e c$  and  $\omega_{ci} = eB_0/m_i c$  are defined with the initial magnetic field value at the upstream boundary. Then, the electron gyro-radius is defined as  $\rho_e = v_{Te}/\omega_{ce}$ , and the ion gyroradius  $\rho_i = v_{Ti}/\omega_{ci}$ . The Alfvén velocity  $V_A = B_0/(4\pi n_{eb}m_i)^{1/2}$  is defined with the initial magnetic field and the plasma density at the upstream boundary, and the ion plasma beta at the upstream boundary is  $\beta_i = 4\pi n_{eb}T_i/B_0^2$ . The simulations were performed with the following initial input parameters:  $m_i/m_e = 100$ ,  $T_i/T_e = 1$ ,  $\omega_{pe}/\omega_{ce} = 4$ ,  $n_{eb}/n_{e0} = 0.22$ , the time step  $\omega_{ce}\Delta t = 0.02$ , and the spatial grid size  $\Delta x = \Delta y = \lambda_{De}$ . Then,  $v_{Te} = 0.1416c$ ,  $\lambda_{De} = 0.0354c/\omega_{ce}$ ,  $\rho_e = 0.1416c/\omega_{ce}$ ,  $\rho_i = 1.416c/\omega_{ce}$ ,  $\lambda_{di} = 2.46c/\omega_{ce}$ ,  $V_A/c = 0.0533$ , and  $\beta_i = 0.32$ . The driving electric field at the upstream boundary is chosen to be uniform on the upstream boundaries with  $E_{z0}/B_0 = -0.04$  after  $\omega_{ce}t = 335$ . Thus, the  $E \times B$  drift velocity ( $V_d/V_A = cE_{z0}/V_A B_0 = 0.75$ ) is smaller than the electron thermal velocity, but is larger than the ion thermal velocity. The simulation box size  $L_x \times xL_y$  in the  $(x, y)$  poloidal plane is varied from  $(40c/\omega_{ce}) \times (9c/\omega_{ce})$  to  $(68c/\omega_{ce}) \times (18c/\omega_{ce})$  to make sure that the boundaries do not affect the simulation results. The total number of finite-sized particles is on the order of  $10^9$ . In the figures of simulation results shown in the paper, the time is normalized by  $\omega_{ce}^{-1}$ , the distance is normalized by  $c/\omega_{ce}$ , the velocity is normalized by the speed of light  $c$ ,

the electric field and magnetic field are normalized by  $B_0$ , the particle density is normalized by  $n_{e0}$ , the particle pressure tensor is by normalized by  $n_{e0}m_e c^2$ , and the current density is normalized by  $B_0\omega_{ce}/c$ . In the paper the simulation results are shown for the time of  $\omega_{ce}t = 653.84$  when the reconnection rate reaches quasi-steady.

## 3. Decoupling of Electron and Ion Dynamics

The most important kinetic physics of magnetic reconnection is the decoupling of electron and ion dynamics around the magnetic field reconnection region and near the field line separatrix. When oppositely directed magnetic fields are driven by the inductive electric field  $\vec{E}_z$  to merge toward the neutral sheet to reconnect, both the electrons and ions drift together with the magnetic field. However, around the reconnection layer, the electron and ion flow dynamics decouple and are substantially different. Electrons flow from the upstream region mainly through the magnetic field reconnection region into the downstream region as shown in Fig. 1 (a). In the upstream side of the separatrix, electrons flow mainly along the field line toward the immediate upstream region just outside the reconnection region. Although some ions flow through the reconnection current layer into the downstream, most ions flow across the field line separatrix into the downstream as shown in Fig. 1 (b). The electron outflow velocity from the reconnection region dominates over the ion outflow velocity in the current layer and the downstream exhaust region, and thus a pair of currents flow inward toward the reconnection region in the reconnection plane. The pair of inward flowing currents generate the out-of-plane quadrupole magnetic field  $B_z$  which concentrates mainly around the separatrix regions as shown in Fig. 2 (a). The total magnetic field strength is shown in Fig. 2 (b).

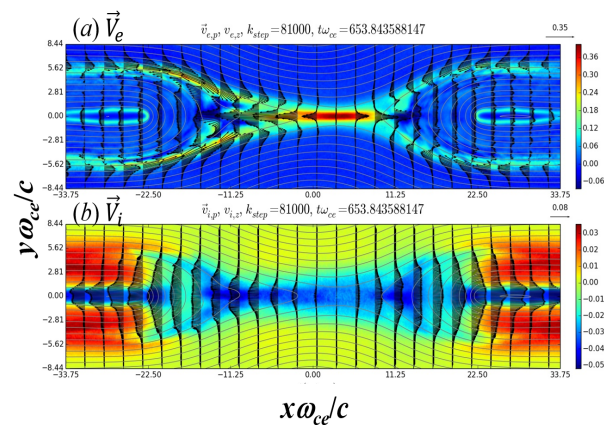


Fig. 1 Poloidal distributions of (a) the electron flow velocity, and (b) the ion flow velocity. Arrows indicate the poloidal flow components and colors indicate the flow  $z$ -components. The contours are the poloidal field lines.

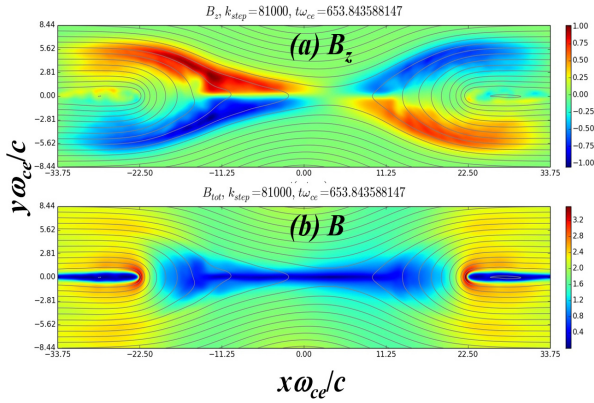


Fig. 2 Poloidal distributions (in color) of (a) the quadrupole magnetic field  $B_z$  and (b) the total magnetic field  $B$ .

It should be pointed out that although the Hall current was first discussed by Sonnerup [3] based on the Hall-MHD model, however, the physical mechanism of how the currents flow from the downstream region into the reconnection region in the kinetic models is totally different from the Hall-MHD model. Thus, the physical mechanism of how this current is produced has continued to be debated. In the driven magnetic reconnection paper of Cheng *et al.* [1], we clearly explained the physical mechanisms of why the electron outflow velocity from the reconnection region reaches super Alfvénic speed and then decreases to Alfvén speed further downstream. The fast electron outflow in the reconnection region is related to the electron flat-top field-aligned velocity distribution (mainly in the  $v_x$  direction) in the immediate upstream of the reconnection current layer. The electron flat-top field-aligned velocity distribution is formed by electrons accelerated by the parallel electric field along field lines outside the separatrix toward the immediate upstream region of the reconnection current layer. Note that our physical mechanism of how electrons are accelerated by the parallel electric field near the separatrix is different from that proposed by Uzdensky and Kulsrud [4] who made use of the argument of changes in the flux tube volume to explain the electron parallel flow near the separatrix. Our physical mechanism of how electrons are accelerated toward the reconnection region along the field line around the separatrix region is also different from the electron surfing mechanism by Hoshino [5] which did not consider the parallel electric field effect.

As the flat-top field-aligned velocity distribution electrons enter the reconnection current layer, they also gain out-of-plane velocity ( $v_z$ ) due to  $E_y B_x / B^2$  drift by the electrostatic bipolar electric field  $E_y$  in the region outside the electron orbit meandering width (but inside the ion meandering width) and by the reconnecting electric field  $E_z$  acceleration inside the electron orbit meandering region. The cyclotron turning of the electron ( $v_x, v_z$ ) velocity by the Lorentz force to the outflowing  $x$ -direction is small inside

the reconnection current layer because the vertical magnetic field  $B_y$  is weak so that the electron outflow velocity is mainly determined by the flat-top  $v_x$ -velocity distribution. Thus, inside the reconnection current layer the electron outflow velocity reaches super-Alfvénic speed and is much larger than the  $E_z B_y / B^2$  drift velocity except near the X-point where the magnetic field is very weak. This physical mechanism is different from the undriven kinetic magnetic reconnection simulation results of Chen *et al.* [6] in which the electron outflow from the reconnection current layer is explained in terms of the cyclotron turning of the meandering electron out-of-plane velocity ( $v_z$ ) by the vertical magnetic field  $B_y$  into the outflow direction while the meandering electron out-of-plane velocity ( $v_z$ ) is accelerated by the inductive electric field.

It is worthwhile to point out that Hoshino *et al.* [7] and Shay *et al.* [8] explained the super Alfvénic electron outflow velocity based on the concept of  $E \times B$  drift velocity of electrons and ions when their dynamics become magnetized at different distances ( $\Delta_e$  and  $\Delta_i$ , respectively) from the X-point. At  $x = \Delta_i$  where ions are magnetized, the ion outflow velocity is assumed to be the Alfvénic speed  $V_{ix} = |E_z / B_y(\Delta_i)| = V_A$ . By assuming that the vertical magnetic field is approximated by  $B_y(x) = B_y(\Delta_i)(x/\Delta_i)$  and the reconnecting electric field  $E_z$  is uniform, the electron outflow velocity at  $x = \Delta_e$  is taken to be the  $E \times B$  drift velocity  $V_{ex} = |E_z / B_y(\Delta_e)| = V_A(B_y(\Delta_i) / B_y(\Delta_e)) = V_A(\Delta_i / \Delta_e)$ . The size of the unmagnetized region for charged particles from the X-point is estimated by assuming that the particle gyroradius in the local magnetic field equals to the distance from the X-point. Thus,  $\Delta_i = V_A(m_i c / e B_y(\Delta_i))$  and  $\Delta_e = V_{ex}(m_e c / e B_y(\Delta_e))$ . Then,  $\Delta_i / \Delta_e = (m_i / m_e)^{1/3}$  and the electron outflow velocity is given by  $V_{ex} = V_{Ae}(m_e / m_i)^{1/6}$  where  $V_{Ae} = V_A(m_i / m_e)^{1/2}$  is the electron Alfvén speed. This explanation does not apply to the fast electron outflow speed in the unmagnetized electron region  $x < \Delta_e$  and the outward increasing ion outflow speed in the unmagnetized ion region  $x < \Delta_i$ .

From our driven reconnection simulation results shown in Fig. 8 of Cheng *et al.* [1], due to the inflowing electrons with flat-top field-aligned velocity distribution, the electron outflow speed increases rapidly to super Alfvénic speed and then decreases to the  $E \times B$  drift speed at  $x = \Delta_e = 7c / \omega_{ce}$ . However, the electron outflow speed at  $x = \Delta_e$  is much smaller than the electron Alfvén speed  $V_{Ae}$  as argued by Hoshino *et al.* [7]. We have also shown that the ion outflow velocity increases gradually to the  $E \times B$  drift speed (about the value of Alfvén speed) at  $x = \Delta_i = 13c / \omega_{ce}$  as they flow out from the reconnection region into the downstream. The ratio  $\Delta_i / \Delta_e$  is smaller than the theoretical value of  $(m_i / m_e)^{1/3}$  proposed by Hoshino *et al.* [7]. The increase of ion outflow speed is associated with the parallel electric acceleration inside the ion orbit meandering width region [1]. We will not repeat the description of these physical mechanisms here. The difference between the electron outflow velocity and the ion out

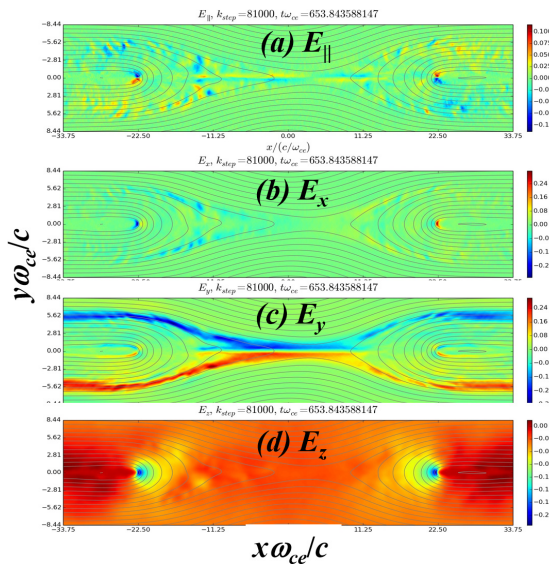


Fig. 3 Poloidal distributions of the electric field in the (a) field-aligned, (b)  $x$ , (c)  $y$ , and (d)  $z$  components.

flow velocity thus creates the large inflow current from the downstream toward the reconnection region. Therefore, the mechanisms of electron and ion outflows in the driven reconnection case have nothing to do with the Hall term in the Hall-MHD Ohm's law, which dictates that the electron velocity perpendicular to the magnetic field line is determined by the  $E \times B$  drift velocity.

With the penetration of the inductive electric field  $E_z$  from the upstream boundary into the reconnection region as shown in Fig. 3 (d), the generation of quadrupole magnetic field  $B_z$  causes significant parallel electric field  $E_{\parallel} = \vec{E} \cdot \vec{B}/B$  which is dominant around the separatrix region as shown in Fig. 3 (a). Note that the poloidal electric field around the separatrix region shown in Figs. 3 (b) and 3 (c) is produced due to charge separation resulting from the decoupling of electron and ion dynamics. Thus, the poloidal electric field is mainly electrostatic in nature and is mainly perpendicular to the ambient magnetic field because fast moving electrons will try to smear out the large scale charge separation along the field line. The mechanism of how the electrostatic electric field is produced around the separatrix region will be discussed in the later paragraph.

To understand how the parallel electric field is produced, we show the contribution from the inductive electric field and the poloidal electric field separately by decomposing  $E_{\parallel} = E_{\parallel z} + E_{\parallel p}$ , where  $E_{\parallel z} = E_z B_z/B$  and  $E_{\parallel p} = (E_x B_x + E_y B_y)/B$ . Figure 4 shows the poloidal distribution (in color) of (a)  $E_{\parallel z}$  and (b)  $E_{\parallel p}$ . Two poloidal magnetic field lines around the upper-right separatrix region are also shown in Fig. 4. Figure 5 shows  $E_{\parallel}$  and  $E_{\parallel z}$  and  $E_{\parallel p}$  along (a) the downstream field line inside the separatrix and (b) the upstream field line outside the separatrix shown in Fig. 4. It is clear from Fig. 5 that  $E_{\parallel z}$  and  $E_{\parallel p}$  have op-

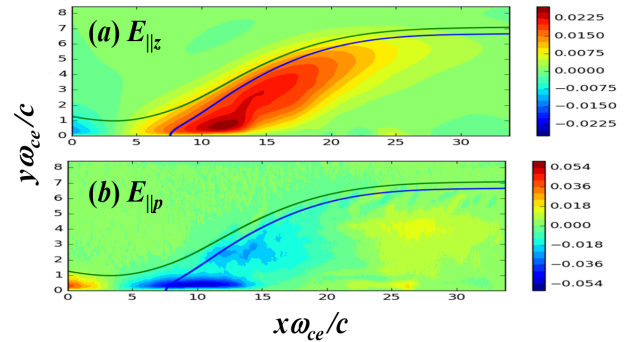


Fig. 4 Poloidal distributions (in color) of (a)  $E_{\parallel z} = E_z B_z/B$  and (b)  $E_{\parallel p} = (E_x B_x + E_y B_y)/B$ . Two poloidal magnetic field lines around the separatrix are shown.

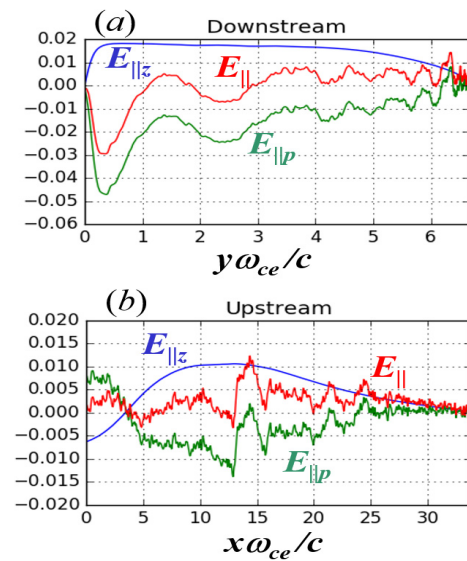


Fig. 5 Variations of the parallel electric field  $E_{\parallel}$  and its contributions from  $E_{\parallel z} = E_z B_z/B$  and  $E_{\parallel p} = (E_x B_x + E_y B_y)/B$  along the poloidal magnetic field lines for (a) the downstream field line inside the separatrix and (b) the upstream field line outside the separatrix shown in Fig. 4.

posite sign. Along the upstream fieldline  $E_{\parallel}$  is mainly due to  $E_{\parallel z}$  and thus the inductive electric field  $E_z$  outside the separatrix ( $x > 5c/\omega_{ce}$ ). Note that the X-point is located at about ( $x = 3.5c/\omega_{ce}$ ,  $y = 0$ ). Along the downstream fieldline  $E_{\parallel}$  is mainly due to  $E_{\parallel z}$  away from the downstream exhaust ( $y > 3c/\omega_{ce}$ ) where the poloidal electrostatic field oscillation amplitude is small, but is dominated by  $E_{\parallel p}$  around the outflow exhaust region ( $y < 1c/\omega_{ce}$ ). The small scale variations in  $E_{\parallel}$  are associated with high frequency electrostatic waves in the poloidal electric field. Thus,  $E_{\parallel}$  is mainly contributed by the inductive electric field  $E_z$  around the separatrix region, and  $\vec{E}_{\parallel}$  points mainly outward from the reconnection region toward the downstream direction.

It is important to note that the parallel electric field has been discussed in the papers studying undriven magnetic

reconnection [e.g., 5-12]. However, the important issue is how and where the parallel electric field is produced. In the undriven reconnection simulation cases, the generation of parallel electric field is completely different in nature from the driven reconnection simulation case and is mainly due to electrostatic field along the poloidal magnetic field line. In the paper of Egedal *et al.* [9], the parallel electric field exists around the magnetic reconnection region and is due to the trapped electrostatic potential distribution in the poloidal plane and thus the parallel electric field is produced by the poloidal electrostatic electric field in the poloidal magnetic field direction. In the work of Egedal *et al.* [10], the parallel electric field is also electrostatic in nature and is located mainly inside electron density cavities which are along all 4 separators on the downstream side and travel downstream with the exhaust. Within these cavities, strong alternating parallel electric field are observed, which is a signature of electron holes. The alternating parallel electric field has an averaged parallel electric field pointing away from the reconnection region. In the work of Fujimoto [11], the parallel electric field is due to an electrostatic potential hump formed in the inflow side of the separatrices. In the most recent undriven reconnection paper of Fujimoto and Takamoto [12], the parallel electric field contribution by the out-of-plane electric field in the downstream region was almost cancelled out by the in-plane electrostatic electric field. Thus, the total parallel electric field is almost zero in the downstream region. Thus, the generation mechanism of parallel electric field in the undriven magnetic reconnection simulations is due to electrostatic electric field. From the above discussion, we also wonder why the parallel electric field generation mechanisms presented in these undriven reconnection simulation papers are all different. This should be studied in the future.

The electrons are accelerated by  $E_{\parallel}$  in the direction opposite to the  $E_{\parallel}$  direction. As shown in Fig. 1 (a), on the upstream side and around the separatrix field lines electrons are accelerated to flow very fast along the field lines toward the reconnection region direction. However, on the field lines just inside the separatrix the inward accelerated electrons are balanced with the outflowing electrons so that the field-aligned flow velocity is small. Further toward the midplane from the separatrix the electron outflow velocity is mainly contributed by the outflowing electrons because  $E_{\parallel}$  which accelerates electrons toward the reconnection region direction becomes much weaker.

On the other hand, due to large ion mass the ion parallel flow velocity due to acceleration by the parallel electric field around the separatrix region is smaller than the  $E \times B$  drift velocity and thus ions flow mainly across the field line into the downstream as shown in Fig. 1 (b). Then, the electron density must be smaller than the ion density on the upstream side of the separatrix so that the net charge is positive. In the downstream side of the separatrix, the combination of fast outflowing electrons and electrons drifting

across the field line into the downstream side have higher density than the density of ions drifting across the separatrix to the downstream side of the separatrix. Thus, on the downstream side of the separatrix the net charge is negative. Thus, the ion flow dynamics decouples from the electron flow dynamics around the separatrix region. This decoupling of electron and ion flow dynamics produces net positive (negative) charge on the upstream (downstream) side of the separatrix, and thus an electrostatic electric field is produced in the poloidal plane with  $E_x$  and  $E_y$  shown in Figs. 3 (b) and 3 (c). Note that around the separatrix regions the electrostatic electric field is mainly perpendicular to the ambient magnetic field and points toward the downstream mid-plane direction.

As shown in Figs. 3 (b) and 3 (c) a pair of bipolar electrostatic electric fields (mainly  $E_y$ ) is produced around the neutral sheet region where the merging magnetic field lines reconnect. The bipolar electrostatic electric field is quite large and is produced by the decoupling of the electron and ion orbits due to orbit meandering motion, which is different from the decoupling mechanism around the separatrix regions.

Around the field reversal region, their orbit motion perpendicular to the magnetic field becomes meandering because the magnetic field is weakened and reversed across the neutral sheet [13]. The particle gyroradius  $\rho(y) = v(y)/\omega_c(y)$ , where  $v$  is the particle velocity perpendicular to the magnetic field and  $\omega_c = eB/mc$  is the gyrofrequency, changes with the particle distance  $y$  from the neutral sheet. The orbit meandering width scale is determined by  $\Delta_m = \rho(y = \Delta_m)$ , when the local particle gyroradius equals to the local magnetic field gradient scale length  $\rho(y) = |\partial \ln B / \partial y|^{-1}$ . For example, for  $B = yB_0/L$  and  $\rho_0 = v/(eB_0/mc)$  the particle orbit meandering width is  $\Delta_m = (\rho_0 L)^{1/2}$ . Because  $m_i \gg m_e$ , the ion meandering width  $\Delta_{mi}$  is larger than the electron meandering width  $\Delta_{me}$  and their ratio is  $(T_i m_i / T_e m_e)^{1/4}$  for thermal particles [13]. Inside the orbit meandering region particles un-magnetized and can be accelerated or decelerated by the perpendicular electric field depending on the ion velocity direction with respect to the perpendicular electric field, but are always accelerated by the parallel electric field. Therefore, the electron and ion orbit motions are decoupled inside the ion meandering region.

As particles drift toward the neutral sheet the particle density increases. Inside the orbit meandering region, the particle density accumulates and is roughly uniform. Thus, the ion density is larger (smaller) than the electron density outside (inside) the electron orbit meandering region. The charge separation produces a pair of in-plane bipolar converging electrostatic electric field pointing toward the neutral sheet (shown in Figs. 3 (b) and 3 (c)).

It is worthwhile to mention that the bipolar electrostatic electric field (or called the Hall electric field) around the current layer was first obtained in the Hall-MHD simulations although with different magnitude and structure.

However, the Hall electric field is mainly due to the inductive electric field because the charge quasi-neutrality is strictly imposed in the Hall-MHD model. Thus, the generation mechanism of the Hall electric field in the Hall-MHD model is completely different from the charge separation mechanism obtained from the driven reconnection using the full kinetic PIC model presented in this paper. It is also interesting to point out that different mechanisms of the Hall electric field were presented in previous publications. In Arzner and Scholer [14], they investigated hybrid simulation with particle ions and massless fluid electrons, and they obtained bipolar electric field (shown in Fig. 8 of [14]), but did not explain how the bipolar electric field is generated, but instead stated that the bipolar electric field is balanced with the Hall (out-of-plane) magnetic field from the Ohm's law. In Hoshino *et al.* [7] they showed the full kinetic PIC simulation results with the poloidal electric field magnitude distribution and stated that the polarization electric field is produced by the inertia difference between ions and electrons and referred the interpretation to the paper by Hoshino [15]. The argument given in [15] is that the electron density changes adiabatically in the Hall region, which is defined to be the space extending from an electron inertial length to an ion inertial length from the neutral sheet. In contrast, ions do not behave adiabatically. Therefore, an ambipolar electric field develops in a charge neutral plasma, which causes the ions to accumulate in the neutral sheet. This interpretation is very different from our mechanism based on the charge separation (non-charge neutrality) resulting from the smaller electron orbit meandering region inside the larger ion orbit meandering width region around the neutral sheet presented in this paper. In the PIC simulation study of undriven reconnection by Fujimoto [16], a small difference between the electron and ion density profiles across the neutral sheet is attributed by the mass difference between ions and electrons. Although the ion meandering motion is mentioned, there is no detailed explanation of physical mechanism of how the charge separation is produced. The resulting bipolar electric field is within a factor of 2 of the reconnection electric field. This result is different from the driven reconnection simulation result [1] and the space observation by Wygant *et al.* [17] that the bipolar electrostatic electric field is about one order of magnitude larger than the reconnection electric field. In the PIC simulation work of Drake *et al.* [18], the whole paper discussed the macroscopic quantities calculated from the particle distribution and how these macroscopic quantities affect the flow and current dynamics through the generalized Ohm's law. There was no discussion of the microscopic kinetic process of how the bipolar electric field is produced. In the PIC simulation work of Chen *et al.* [6], the main emphasis is the electron phase space hole structure inside the electron orbit meandering region. There was no discussion on the physical mechanism of how the bipolar electric field is produced. In fact, the electron phase space hole structure inside the electron orbit meandering

region was first published by Horiuchi and Ohtani [19] for the driven reconnection case.

## 4. Summary and Discussion

In this paper we have explained the physical mechanisms of (1) how the quadrupole out-of-plane magnetic field and the parallel electric field are produced, (2) the decoupling of the electron and ion dynamics, and (3) the generation of the charge separation and the in-plane electrostatic electric field. With the understanding of the generation and structure of these electric and magnetic fields, we can understand how electrons and ions are accelerated and heated [1]. In particular, the spatial scale of the electrostatic electric field in the direction perpendicular to the magnetic field in the magnetic reconnection and separatrix regions is comparable to or smaller than the ion gyroradius, thus ions are accelerated not only by the parallel electric field along the field line, but also by the electrostatic electric field in the direction perpendicular to the magnetic field line.

Electrons accelerated by the parallel electric field flow along the field lines from both upstream separatrix regions to the upstream region just outside the reconnection region, where the magnetic field forms a magnetic well as shown in Fig. 2(b), and forms a flat-top parallel velocity distribution with large velocity spread as observed in the magnetotail [20, 21]. Thus, after the electrons move from upstream through the reconnection current layer into the downstream, the parallel velocity spread in the electron flat-top  $v_{\parallel}$ -distribution in the immediate upstream is converted to the perpendicular velocity with large spread around the mean electron perpendicular drift velocity. This is a critical mechanism of how electrons are thermalized and heated in the perpendicular velocity direction in the downstream. Moreover, because of the adiabatic invariant of the electron magnetic moment, the electron velocity distribution in all three velocity directions has large thermal velocity spread, which is larger than the electron mean flow velocity.

The ion dynamics through the current layer into the downstream is determined by the ion orbit meandering effect, the inductive and bipolar electrostatic electric fields, and the change of the magnetic field topology from the upstream to the downstream. When ions move across the field lines into the orbit meandering region, the ions are accelerated (decelerated) by the bipolar electrostatic electric field before (after) they move across the neutral sheet as their orbits become meandering in the field reversal region. The ion inflow velocity is reduced because of the acceleration/deceleration of the orbit meandering ion velocity by the electrostatic electric field, which causes large ion velocity spread. Inside the ion meandering region the ions are directly accelerated by the inductive electric field to gain ion flow velocity in directions both perpendicular and parallel to the magnetic field. The ion outflow velocity

around the reconnection region is contributed mainly by the ion parallel flow velocity.

Around the separatrix region the ion gyroradii are comparable to or large comparing with the electrostatic electric field localization width. As ions move across the separatrix region, the ion orbit gyrates around the magnetic field. The ions do not gain energy from the electrostatic electric field in one orbit gyration, and the ion gyration motion thermalizes the ion velocity in the direction. But, after one orbit gyration the ions are accelerated by the electrostatic electric field to gain energy. In the meantime, the ions are accelerated continuously by the parallel electric field to gain large parallel velocity.

Ions gain both flow kinetic energy and thermal energy in the current layer and the downstream. It is to be emphasized that when ions flow from the upstream through the reconnection current layer or across the separatrix region into the downstream, they gain energy mostly from the inductive electric field, which penetrates to the entire reconnection domain. Only a smaller part of ion energy is gained from the electrostatic field in the downstream separatrix region.

In summary, we have presented physical mechanisms of key driven magnetic reconnection processes in collisionless plasmas in driven reconnection. Many interpretations of the key processes are new and have not been discussed before. Moreover, it is to be noted that our physical interpretation of how the quadrupole magnetic field is generated and how the electron parallel velocity is accelerated by the parallel electric field around the separatrix region are different from the one presented by Uzdensky and Kulsrud [4], who made use of the argument of changes in the flux tube volume to explain the electron parallel flow near the separatrix. Our physical picture of how electrons are accelerated by the parallel electric field along magnetic field lines on the upstream side of the separatrix region is also different from the electron surfing mechanism proposed by Hoshino [5], which did not consider the parallel electric field effect associated with the quadrupole out-of-plane magnetic field generation. Our results of ion acceleration/heating mainly by the inductive electric field are also different from the conclusion drawn in the previous papers [22, 23] that the ions are mainly accelerated by the electrostatic electric field across the field line separatrix into the downstream.

Finally, we have discussed many differences in the kinetic physics between driven and undriven reconnection cases, which has not been discussed previously. However, the reasons for these differences are still not well understood. Moreover, all the major differences must be systematically identified and explained. Thus, it is important to pursue this issue further in the future studies.

- [1] C.Z. Cheng, S. Inoue, Y. Ono and R. Horiuchi, *Phys. Plasmas* **22**, 101205 (2015).
- [2] M. Ohtani and R. Horiuchi, *Plasma Fusion Res.* **4**, 024 (2009).
- [3] B.U.O. Sonnerup, *Magnetic field reconnection*, in *Solar System Plasma Physics*, edited by L.J. Lanzerotti, C. Kennel and E. Parker (North-Holland, New York, 1979), p.45.
- [4] D.A. Uzdensky and R.M. Kulsrud, *Phys. Plasmas* **13**, 062305 (2006).
- [5] M. Hoshino, *J. Geophys. Res.* **110**, A10215 (2005).
- [6] L.-J. Chen, W.S. Daughton, B. Lefebvre and R.B. Torbert, *Phys. Plasmas* **18**, 012904 (2011).
- [7] M. Hoshino, T. Mukai, T. Terasawa and I. Shinoha, *J. Geophys. Res.* **106**, 25979 (2001).
- [8] M.A. Shay, J.F. Drake, B.N. Rogers and R.E. Denton, *J. Geophys. Res.* **106**, 3759 (2001).
- [9] J. Egedal, M. Oieroset, W. Fox and R.P. Lin, *Phys. Rev. Lett.* **94**, 025006 (2005).
- [10] J. Egedal, W. Daughton and A. Le, *Nature Phys.* **8**, 321 (2012).
- [11] K. Fujimoto, *Geophys. Res. Lett.* **41**, 2721 (2014).
- [12] K. Fujimoto and M. Takamoto, *Phys. Plasmas* **23**, 012903 (2016).
- [13] A. Ishizawa and R. Horiuchi, *Phys. Rev. Lett.* **95**, 045003 (2005).
- [14] K. Arzner and M. Scholer, *J. Geophys. Res.* **106**, 3827 (2001).
- [15] M. Hoshino, *J. Geophys. Res.* **92**, 7368 (1987).
- [16] K. Fujimoto, *Phys. Plasmas* **13**, 072904 (2006).
- [17] J.R. Wygant *et al.*, *J. Geophys. Res.* **110**, A09206 (2005).
- [18] J.F. Drake, M.A. Shay and M. Swisdak, *Phys. Plasmas* **15**, 042306 (2008).
- [19] R. Horiuchi and H. Ohtani, *Comm. Comput. Phys.* **4**, 496 (2008).
- [20] Y. Asano *et al.*, *J. Geophys. Res.* **113**, A01207 (2008).
- [21] J. Egedal *et al.*, *J. Geophys. Res.* **115**, A03214 (2010).
- [22] J. Yoo, M. Yamada, H. Ji and C.E. Myers, *Phys. Rev. Lett.* **110**, 215007 (2013).
- [23] M. Yamada *et al.*, *Nature Comm.* **5**, 4774 (2014), doi: 10.1038/ncomms5774.